Journal of Physics D: Applied Physics

PURPOSE-LED PUBLISHING™

PAPER • **OPEN ACCESS**

Wind tunnel testing and performance modeling of an atmospheric ion thruster

To cite this article: Stefano Trovato *et al* 2025 *J. Phys. D: Appl. Phys.* **58** 015201

View the article online for updates and enhancements.

You may also like

- Mirror-coupled plasmonic nanostructures for enhanced in-plane magnetic dipole emission
Ruizhao Yao, Sheng Lan and Guang-Can Li
- Blade emitters for atmospheric ionic thrusters
M Belan, J Baldo, O Kahol et al.
- Impact of thickness and saturation direction over magnetostatic mode energies and profiles in $Ni_{80}Fe_{20}$ antidots
S Chiroli, D Faurie, A O Adeyeye et al.

This content was downloaded from IP address 131.175.12.9 on 15/10/2024 at 08:27

OPEN ACCESS
IOP Publishing
Journal of Physics D: Applied Physics
J. Phys. D: Appl. Phys. **58** (2025) 015201 (14pp)
https://doi.org/10.1088/1361-6463/ad7d9c

Wind tunnel testing and performance modeling of an atmospheric ion thruster

Stefano Trovato*, **Raffaello Terenzi**, **Davide Usuelli** and **Marco Belan**

Politecnico di Milano, Dipartimento di Scienze e Tecnologie Aerospaziali, 20156 Milano, Italy

E-mail: stefano.trovato@polimi.it

Received 4 July 2024, revised 22 August 2024
Accepted for publication 20 September 2024
Published 14 October 2024

Abstract

In this work a complete atmospheric electro–hydro-dynamic (EHD) thruster is tested in a subsonic wind tunnel, with the purpose of evaluating changes in performance due to simulated flight conditions and, for the first time, comparing them with a physical model of the drift region. An aerodynamic frame was designed to accommodate the electrodes inside the wind tunnel. Propulsive force and electrical measurements were conducted to assess performance exploiting dimensionless coefficients derived from one-dimensional theory. The results, on top of validating the theory, show how EHD thrusters can operate with a non-zero bulk velocity and highlight the importance of optimized frames and electrodes to enhance the capabilities of flying demonstrators. The test campaign revealed that the operating voltage envelope extends with increasing bulk velocity, leading to an increase in maximum thrust.

Keywords: EHD propulsion, atmospheric ion thruster, corona discharge, wind tunnel EHD thruster

1. Introduction

Electric propulsion has emerged as a promising trend in aeronautics, offering potential alternatives to traditional combustion engines, which may be substituted with electric motors or atmospheric ionic thrusters. The latter have been extensively used for space application [1–3], but it is only recently that the scientific community is pushing to deliver a thruster that can be used in atmospheric conditions [4, 5]. Electro–hydro-dynamic (EHD) atmospheric thrusters have the great advantages of being highly efficient in terms of Thrust-to-Power ratio, absence of moving parts, low noise output and low maintenance requirements. In its simplest form, an EHD thruster is composed by two electrodes separated by a distance called gap. The ion emitter is smaller in size and is typically a thin metallic wire with a diameter generally below 200 μm, the ion collector instead is a larger object, often in the shape of a cylinder [6] or an aerodynamic airfoil [7]. A strong electric field is imposed by applying a high voltage difference between the two electrodes through a power source. The intense electric field near the emitter ionizes the gas, initiating a corona discharge [8]. The ions drift towards the collector, transferring their momentum to neutral molecules through collisions. This process creates a ionic wind, through which a net thrust is generated. This effect has been a subject of multiple studies over the last century [9–14]. The aforementioned thruster configuration has already been used in flying prototypes such as [7] and a similar one was used by [15]. All the main geometrical parameters related to spatial arrangement have undergone through different optimization studies including dimensions of the collectors [16] and their spacing [17] and gap selection [18]. These studies aimed at increasing one or more of the main performance indicators of an EHD thruster, such as thrust density (T/A), an index of compactness of the thruster, where

* Author to whom any correspondence should be addressed.

Original Content from this work may be used under the terms of the Creative Commons Attribution 4.0 licence. Any further distribution of this work must maintain attribution to the author(s) and the title of the work, journal citation and DOI.

© 2024 The Author(s). Published by IOP Publishing Ltd

A is a reference area, and thrust-to-power ratio (T/P), an index of efficiency, where P is the power consumption. Another measure is increasing the emitter's density [19], that means placing more than one emitter for each collector, which is beneficial to all performance indicators up to the limit imposed by electrical shielding between the emitters themselves [20, 21]. Another field of investigation is related to ion generation. The electrodes are usually supplied with a high voltage DC power source, however other options are available: ion generation and acceleration can be decoupled [22, 23] so that DBD technology may be used as the ion source; repeating pulses in the nanoseconds range supplied to the electrodes may be exploited to generate a large amount of ions before breakdown occurs [24, 25]. The majority of EHD thrusters uses thin metallic wires as emitting electrodes; however, these wires are fragile and cannot sustain bending loads which can lead to early failure of the system. Increasing the diameter of the wires would increase the robustness of the emitters but, at the same time, it would increase the inception voltage [26], decreasing the performance of the thruster. Different emitters geometry were also tested such as blade emitters [27–29] or pins [30–32].

A fundamental stepping stone to further the advancement of this technology, with the aim of a future application on a flying demonstrator, is the analysis of the thruster's performance in the presence of a convective flow. So far, this problem has only been partially tackled theoretically, as in [33] and [34]. On the experimental side, the only related works, to our knowledge, are [35], albeit centered on a different aspect unrelated to EHD thrusters, and [36], which however lacks a direct measure of thrust, as well as a complete physical model to compare the results. The scope of this article is therefore the experimental investigation of an EHD thruster with the addition of convective velocity. The results will be compared with the latest theoretical predictions by [34], with the inclusion of the performance parameters introduced in [16]. The selected thruster employs the same collectors which were found to be optimal for the Thrust-to-Power ratio according to [16], using the increased anodic density suggested by [19], therefore maximizing also the thrust production. The selected configuration is then incorporated into an aerodynamic frame, suitable to be inserted inside a relatively small low-speed wind tunnel. Force and electric measurements are used to analyze the thruster's performance. The test campaign is also aimed at understanding the operating envelope of the thruster at varying velocities, with particular interest on the ignition and breakdown voltages, both of which are outside the reach of many available theoretical articles, which focus on the drift region. The ionization region is instead of paramount importance for the ignition and breakdown phenomena, it however lacks an analytical model which can be linked to the varying convective velocity.

This paper is organized as follows: in section 2 the theoretical model and performance parameters are discussed, section 3 presents the setup used during the test campaign, section 4 shows and discusses the outcomes of the experimental campaign.

2. 1D theory model & performance parameters

2.1. 1D theory modelling

The results of the experimental campaign shown in section 4 are presented and discussed according to a 1D theory model developed to generate dimensionless performance parameters and to predict the thruster behavior in the presence of a non null convective flow. The model presented here follows the footsteps of the work discussed in [16, 34].

The motion of ions and neutral molecules in the drifting region is governed by a system of EHD equations that are reported here under the assumption of steady 1D incompressible flow:

$$\frac{\mathrm{d}}{\mathrm{d}x}\begin{bmatrix} E \\ j \\ v_\mathrm{b} \\ p \end{bmatrix} = \begin{bmatrix} \rho_\mathrm{q}/\epsilon \\ 0 \\ 0 \\ \rho_\mathrm{q} E \end{bmatrix} \tag{1}$$

where E is the electric field, ρ_q the charge density, ϵ the permittivity, v_b and p the hydrodynamic velocity and pressure. The current density j can be expressed, neglecting charge diffusion, as

$$j = \rho_\mathrm{q}\left(\mu_\mathrm{q} E + v_\mathrm{b}\right) \tag{2}$$

where μ_q is the ion mobility. The closing equation for the system is:

$$V = \int_0^d E(x)\,\mathrm{d}x \tag{3}$$

where V is the applied voltage and d is the gap between the electrodes.

In this discussion the drifting region domain is defined between $\bar{x} = x/d = 0$ (location of the emitter supplied at $V = V_\mathrm{a}$) and $\bar{x} = 1$ (location of the grounded collector).

The system of equations can be solved for the electric field distribution $E(v_\mathrm{b}, j, x, \rho_{\mathrm{q}0})$,where $\rho_{\mathrm{q}0}$ is the boundary condition for charge density imposed at $\bar{x} = 0$.

$$E(v_\mathrm{b}, j, x, \rho_{\mathrm{q}0}) = \sqrt{\frac{2jx}{\epsilon\mu_\mathrm{q}} + \left(\frac{j}{\mu_\mathrm{q}\rho_{\mathrm{q}0}}\right)^2} - \frac{v_\mathrm{b}}{\mu_\mathrm{q}}. \tag{4}$$

Under the assumption of the space charge limited current ($\rho_{\mathrm{q}0} \to \infty$) and null bulk velocity ($v_\mathrm{b} = 0$) the previous equation simplifies to the well-known Mott–Gurney law.

Equations (3) and (4) can be solved for the current density j once the applied voltage V_a (equivalent to V_c, i.e. the corona voltage, for this case), the bulk velocity v_b and the charge density $\rho_{\mathrm{q}0}$ have been fixed. The relationship between current density and bulk velocity can be presented in their dimensionless form defining $\bar{J} = \frac{j}{j_\mathrm{MG}}$ and $R_\mathrm{v} = \frac{v_\mathrm{b}}{\mu_\mathrm{q} V_\mathrm{a}/d}$ as in [16], where j_MG is the Mott–Gurney current and R_v is the bulk velocity made dimensionless with a characteristic ionic velocity. Figure 1 shows model prediction for different values of $\rho_{\mathrm{q}0}$. As the charge density increases the current density curves collapse onto a single curve. This relationship shows

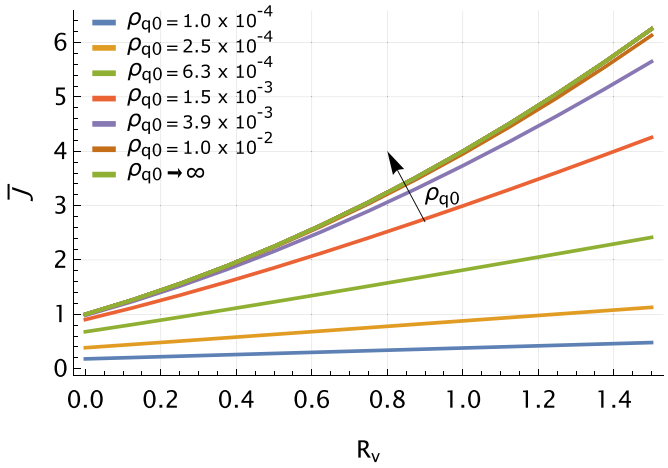

Figure 1. Current density $\bar{J}$ vs dimensionless velocity R_v for different charge densities ρ_{q0} in C/m.

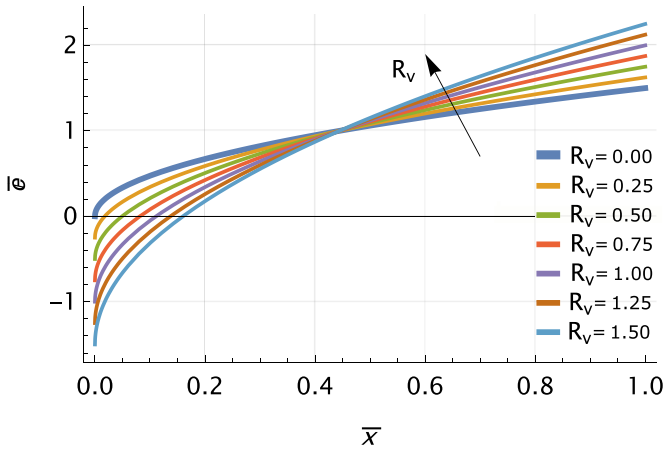

Figure 2. Electric field $\bar{e}(\bar{x})$ for different dimensionless velocity R_v.

a quadratic behavior in accordance with the model developed in [34].

Current density values are used to map the electric field, shown in figure 2, through equation (4) as $\bar{e}(\bar{x}) = \frac{E(\bar{x})}{E_{ref}}$, where the reference electric field is defined as $E_{ref} = \frac{V_a}{d}$. The electric field distribution associated to $R_v = 0$ is highlighted for reference.

Note that, according to this model, the electric field at the emitter E_0 is related to ρ_{q0}:

$$E_0 = \frac{1}{\mu_q}\left(\frac{j}{\rho_{q0}} - v_b\right). \tag{5}$$

Under the assumption of space charge limited current $\rho_{q0} \to \infty$ there may be a negative electric field at the emitter. Moving towards the collector the electric field increases due to the drifting of positive ions.

The charge density distribution can be computed according to equation (6):

$$\rho_q(v_b, j, x, \rho_{q0}) = \frac{j}{\mu_q E(v_b, j, x, \rho_{q0}) + v_b}. \tag{6}$$

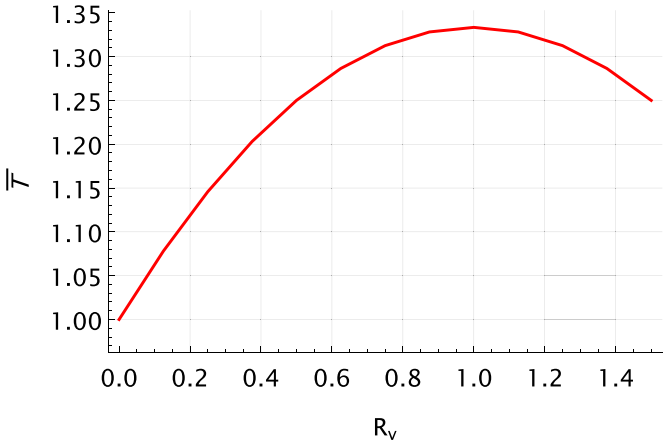

Figure 3. Dimensionless thrust as a function of dimensionless bulk velocity.

The obtained field distributions are used to predict the performance parameters of the thruster under the hypothesis of space charge limited current $\rho_{q0} \to \infty$. First, the EHD thrust is computed according to its definition:

$$T_{EHD} = \int_0^d \rho_q(x) E(x) \, dx \tag{7}$$

and then plotted in dimensionless form as $\bar{T} = \frac{T_{EHD}}{T_{EHD, R_v=0}}$:

Figure 3 shows the thrust behavior with respect to the convective velocity. The curve has a maximum that occurs when the drifting velocity of the ions becomes comparable with the bulk velocity, $R_v = 1$. While this curve has been retrieved numerically, it can be shown that it is actually a parabola, as proven by [34].

Finally the efficiency of the thruster expressed as a thrust-to-power ratio T/P, where P is the power consumption, is obtained and made dimensionless as $\bar{\Theta} = \frac{T/P}{T/P_{,R_v=0}}$ and shown in figure 4:

The efficiency is expected to decrease as bulk velocity increases according to this model, its analytical function being that of an hyperbola [34].

The assumption of a space charge limited current (also present in [34]) is reflected in a charge density that goes to infinity near the emitter, which would appear to be non-physical, however the model shows how even modest charge densities near the emitter lead to similar values of current densities and therefore also of the electric field. A different choice for the charge density at the emitter (which is a boundary condition) would therefore only affect the absolute value of thrust, but its trend with velocity would remain unaffected, which is the reason why the 1D model has been developed in the first place. Given the disparity in dimensions, the model could not be used to predict an absolute value for thrust and therefore its value has been normalized (at zero velocity) in order to be compared with the experimental results, retaining however its trend with velocity. It should also be noted that the space charge phenomenon is what limits ions production also in a real thruster, albeit its specific impact (in charge density near

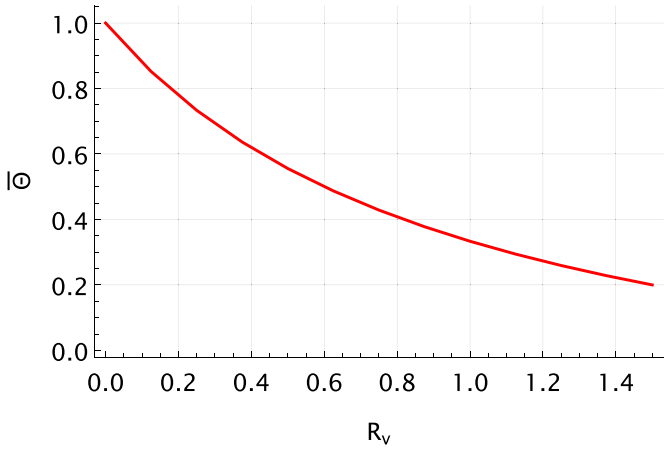

Figure 4. Thrust-to-power $\bar{\Theta}$ vs dimensionless velocity R_v.

the emitter for example) is obviously dictated by the actual geometry and the value of the electric field which is required for ionization; these are not modeled in this 1D model, which lacks the ionization process entirely.

2.2. Dimensionless performance parameters

The level of performance of an EHD thruster is usually presented in terms of generated thrust T, thrust-to-power ratio T/P, which is an index of efficiency, and thrust density T/A, which is an index of compactness. An additional quantity useful to understand the physics of the phenomenon is the corona current i_c that is related to power consumption. In this study the Thrust density is not considered since the setup is the same for all tests, so that T/A can be obtained by scaling the trust with a reference area A.

In this section dimensionless performance parameters are presented: these, contrary to their dimensional counterparts, allow for a better results analysis and provide a meaningful comparison even if different setups are used.

The fundamental quantities to compute from which all parameters can be derived are thrust and power consumption. In this framework they are expressed per unit span and are defined as follows:

$$\frac{T}{b} = \int_{\Omega} \rho_q E_x \, d\Omega \tag{8}$$

$$\frac{P}{b} = \int_{\Omega} j E_x \, d\Omega \, , \tag{9}$$

with Ω being the integration domain, namely the space between the electrodes. Their dimensionless form, presented in table 1, requires reference values for ρ_q, E_x and j that can be computed starting from the system of equation (1). The complete derivation can be found in [16]. The dimensionless coefficient is then retrieved by dividing the dimensional quantity by the corresponding reference value.

Here $\Delta V = V_c - V_i$, where V_i is the ignition voltage. The introduction of ΔV is a modification of the theory in [16] to account for the ignition voltage required for the discharge to develop. V_i has been retrieved experimentally for each test case. While this modification does not interfere with the model in any way, it allows to directly compare the experimental results with the model's predictions. This is necessary as the 1D model only deals with the drift region and therefore does not account for the ionization process, which would be needed to estimate an ignition voltage.

Table 1. Dimensionless coefficients for EHD variables.

Variable	Reference value	Dimensionless quantity
ρ_q	$\epsilon \frac{\Delta V}{d^2}$	$\bar{\rho_q}$
E	$\frac{\Delta V}{d}$	$\bar{e}$
j	$\frac{9}{8}\epsilon \mu_q \frac{\Delta V^2}{d^3}$	$\bar{J}$

As shown before, the electric field varies continuously along the axial direction between the two electrodes, with a particularly high slope near the emitter. Therefore, using $\frac{\Delta V}{d}$ as the reference electric field to define dimensionless parameters might not be the best option.

In fact, in section 4 which is devoted to results presentation, a direct comparison of the laboratory data with the 1D model could be attempted, but it would be unsatisfactory; this reveals an intrinsic limitation of the 1D model in representing data from a physical system that is actually 3D. For this reason, a simple modification of the original model is proposed, introducing a parameter η which leads to a new reference electric field:

$$E_{ref} \longrightarrow \eta E_{ref}.$$

This heuristic assumption, which corresponds for $\eta < 1$ to a relaxation of electric gradients in a 3D geometry, proved to provide a better representation of the experimental data. More specifically, the electric field may change, according to a 1D model, exclusively due to the presence of electric charges, while a real 3D or even 2D setup would have an electric field that is variable also due to geometry. A value of less than unity for η is required to match the experimental results and its physical interpretation is that the effective electric field would be lower in most of the gap of a real 3D thruster, compared to a 1D configuration. And this becomes obvious if the trend of a 2D electric field between a small emitter and a large collector is considered: it would have high values exclusively near the emitter and it would sharply decrease while moving towards the collector. Therefore, for the majority of the drift region, which is where most of the collisions with neutral molecules are taking place (and therefore where the majority of thrust is produced) the electric field of a 2D or 3D geometry is lower than in a 1D case, hence the value of less than unity for the extra parameter that corrects the reference electric field.

Assuming a simplified approach with constant η (which could depend on v_b in a refined model), the performance

Table 2. Performance parameters and dimensionless coefficients.

Name	Symbol	Reference value from [16]	New reference value	Dimensionless coefficient
Thrust	$\frac{T}{b}$	$\epsilon\frac{V_a^2}{d}$	$\epsilon\eta\frac{\Delta V^2}{d}$	C_T
Electrical power	$\frac{P}{b}$	$\mu_q\epsilon_0\frac{V_a^3}{d^2}$	$\mu_q\epsilon_0\eta^2\frac{\Delta V^3}{d^2}$	C_P
Thrust to power	$\frac{T}{P}$	$\frac{d}{\mu_q V_a}$	$\frac{d}{\mu_q\eta\Delta V}$	$C_{TP}=\frac{C_T}{C_P}$
Current	i_c	$\frac{9}{8}A\epsilon\mu_q\frac{V_a^2}{d^3}$	$\frac{9}{8}A\epsilon\mu_q\eta^2\frac{\Delta V^2}{d^3}$	C_C
Velocity	v_b	$\frac{\mu_q V_a}{d}$	$\eta\frac{\mu_q V_a}{d}$	R_v

parameters and scaled velocity in dimensionless form can be defined using the new reference values as shown in table 2, where they are also compared to the ones defined in [16].

It is worth noting that the introduction of η is a simplification of the actual physics of the problem as such a perfect match between the modified 1D model and experimental data should not be expected.

3. Wind tunnel facility and measurement techniques

3.1. Thruster configuration

The experimental campaign was conducted in a general purpose wind tunnel. The facility features a closed-circuit configuration, where the airflow is accelerated through a converging section characterized by a contraction ratio equal to 3. The test chamber presents a rectangular cross section of 300 $\times$ 450 mm, which extends for 1000 mm along the flow direction. In the return section, the airflow is driven by a single-stage axial rotor with a diameter or 630 mm, which in turn is powered by a 6.2 kW asynchronous electric motor, able to provide a maximum velocity of 36.5 m s^{-1} in the test section (figure 5).

In order to investigate the airflow effect on the EHD thruster performance, a structure intended to be mounted in the wind tunnel test section was designed, as illustrated in figure 6. The assembly, which is composed by a structural frame and the thruster units, allows for thrust measurements through the connection to a single monoaxial load cell characterized by a 0−50 N range and an uncertainty of $\pm$ 1 mN. The frame main purpose is to transfer the loads generated by the high-voltage electrodes to the force transducer. Furthermore, the design is intended to reduce aerodynamic drag and prevent the generation of lift and aerodynamic moments that could interfere with the load measurements. As a consequence, all the frame component which are exposed to the wind tunnel airflow are designed as symmetrical streamlined bodies, set at a null angle of attack relative to the mean flow.

The supporting structure includes two sidewalls characterized by a series of holes which allow for a fixed but precise housing of the electrodes, according to the gap and spacing required by the experiment. Each sidewall is composed of a polymethyl methacrylate (PMMA) rectangular cross section, at the edges of which the leading and trailing edges of an acrylic styrene acrylonitrile (ASA) NACA0014 airfoil are mounted, leading to an overall length of 100 mm, thus ensuring the displacement of the emitters and collectors separated by a gap d of 20 mm.

The sidewalls are connected by an ASA bar on the upper end and a rectangular plate on the lower side: while the former—which features NACA0015 cross section due to being located inside the test section—increases the structural rigidity of the setup, the latter is located outside of the test chamber in order to connect the rest of the structure to the load cell and decrease the wetted area. As a consequence, the test section floor features two slots from which the sidewalls pass through.

The thruster itself is composed of 6 collector and 13 emitter electrodes units. The collectors consist in 3D printed NACA0024 airfoils made of ASA characterized by a chord of 25 mm and coated by an aluminum foil of thickness equal to 70 μm. The collector units are mounted on the sidewalls through designated slots at a vertical distance (i.e. spacing) of 35 mm between each other, denoted as s (figure 7). At the intersection between each collector and the supporting frame, an ASA protection is inserted in order to improve electrical insulation and prevent undesired end effects due to the increased electric field intensity in this particular area, providing an effective collector span equal to 243 mm. Moreover, in order to mitigate the increase in aerodynamic drag due to interference, these caps are designed as wing root fairings.

The emitters are constituted by a bare copper wire with a diameter of 100 μm which is wound into a serpentine through designated holes drilled on the sidewalls, leading to an emitter span equal to 270 mm. The emitter configuration is characterized by an internal spacing $h_i = s/2$ equal to 17.5 mm from the first to the last collector and a spacing of 7.5 mm for the two outer wires, denoted as h_e. Collectors thickness ratio as well as the ratio between emitters and collectors and relative spacing were based on the results found in literature [19] and internal studies aimed at increasing thrust density, in order to provide a higher signal-to-noise ratio for the load cell compared to the one deriving from the typical 1 : 1 ratio.

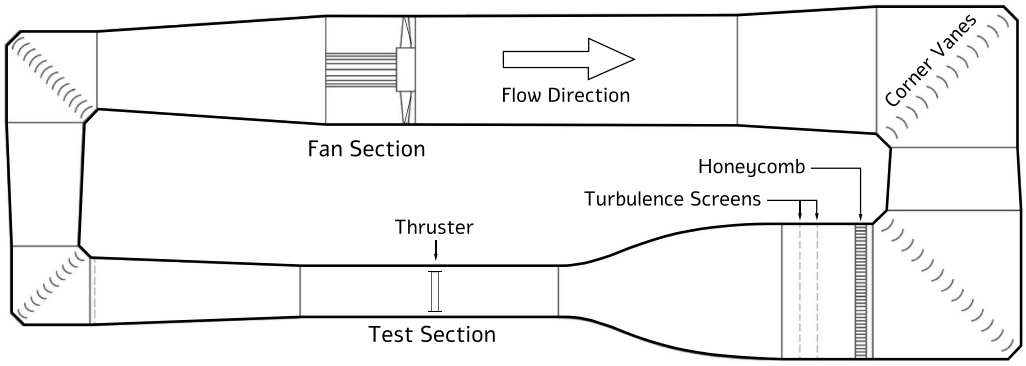

Figure 5. Wind tunnel representation.

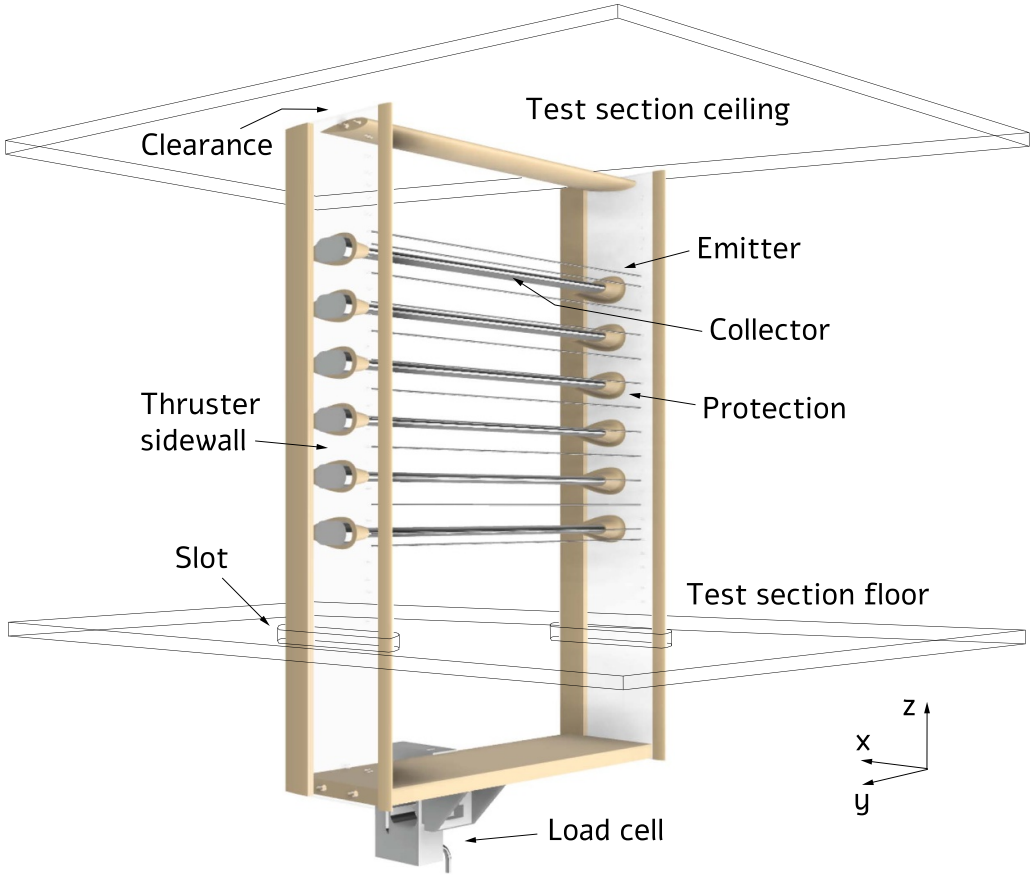

Figure 6. Setup for thrust measurements. The active part of the thruster is exposed to the airstream in the test section, whereas the load cell is located outside the section and shielded from EM disturbances. The load is completely transmitted to the cell through the slots in the floor without any other mechanical connection.

The complete electric setup is shown in figure 8. The high voltage between the electrodes is provided by a purposely built power supply unit, capable of providing a positive DC voltage V_s up to 30 kV. The high voltage generator is in turn composed by a function generator providing a sinusoidal waveform to an audio amplifier that drives a high-voltage transformer. The high-voltage output is then rectified and multiplied by a Cockroft–Walton stage. In order to protect the instrumentation in the event of a short circuit, a ballast resistance R_b of 475 kΩ is placed in series with the thruster. During the experimental campaign, electrical parameters such as voltage V_c and current i_c flowing through the electrodes were measured to calculate the overall power consumption and derive performance indicators.

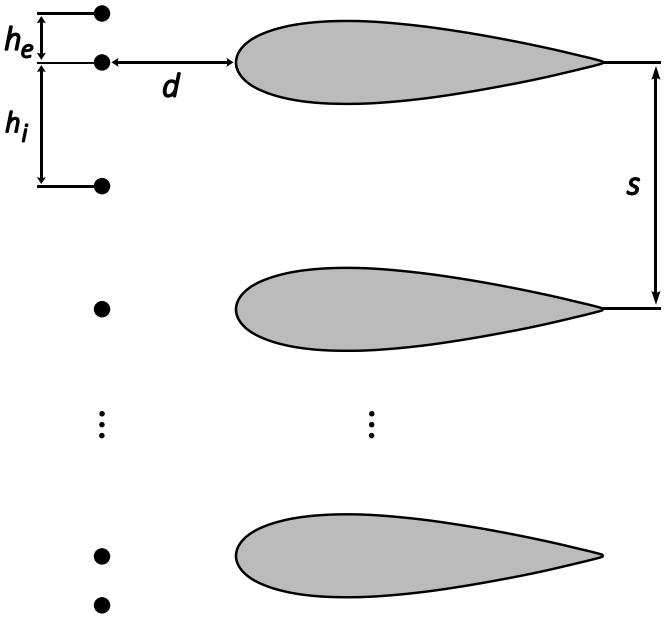

Figure 7. Graphical representation of the electrodes geometric parameters (not to scale).

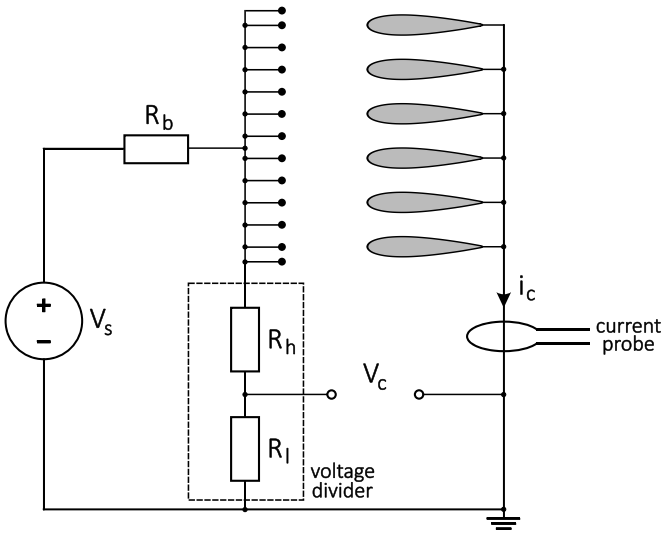

Figure 8. Electrical scheme of the wind tunnel setup.

3.2. Measurements techniques

3.2.1. Velocity measurement. The wind tunnel flow speed v_b is obtained from the relationship derived from Bernoulli's theorem reported here below:

$$v_b = \sqrt{\frac{2K\Delta p}{\rho}} \tag{10}$$

where ρ is the airflow density in the test section, K is the calibration coefficient of the wind tunnel and Δp is the differential static pressure across the converging section, measured by a pressure transducer characterized by a range from 0 to 1 mbar and an uncertainty of 0.1% of the full scale. The calibration coefficient K is dictated by the relationship between the dynamic pressure in the test section and the differential static pressure across the converging section Δp. Previous analyses on the calibration of the wind tunnel revealed that the calibration coefficient K remains virtually constant, consistently at 1.22, across the velocity range analyzed in this study. This approach eliminates the need for a Pitot tube in the test section, thus preventing further disturbances. The airflow density ρ is computed under the hypothesis of ideal gas:

$$\rho = \frac{p}{\mathcal{R}\mathcal{T}} \tag{11}$$

where static pressure p corresponds to the one measured at the exit of the converging section, while the temperature $\mathcal{T}$, which is assumed constant along the circuit, is read in the wind tunnel return leg by a Pt100 temperature probe with a sensitivity of 0.2 K.

3.2.2. Load measurement. The propulsive force is measured by the load cell connected to the lower end of the structural frame. In order to cancel out bending moments that the load cell experiences due to the experimental setup weight, the output signal is preventively set to zero before each acquisition campaign. The net generated thrust, denoted as T, is determined by the difference between the load cell readings when the thruster is electrically switched off (F_{off}) and when it is turned on (F_{on}):

$$T = F_{on} - F_{off}. \tag{12}$$

When the wind tunnel is operational, the term F_{on} includes the contribution of the aerodynamic resistance of the whole model D_{tot} due to the frame, the electrodes as well as turbulence and solid blockage effects:

$$F_{on} = D_{tot} + T. \tag{13}$$

As a consequence of the presence of aerodynamic drag, a variable denominated as effective thrust T_{eff} is introduced. This parameter, defined as the disparity between the total force registered by the transducer and the sole aerodynamic drag of the frame D_{frame}, may be viewed as a first approximation of the behavior of a thruster characterized by an infinite span deprived of the supporting frame:

$$T_{eff} = F_{on} - D_{frame}. \tag{14}$$

The approach described above assures that the determined thrust remains unaffected by the drag of the support structure, which is subject to arbitrary design. Furthermore, the definition leads to an estimation of the overall force as the combined effect of electrohydrodynamic thrust and electrodes aerodynamic drag. Therefore, the effective thrust provides insights into whether the thruster can successfully overcome its inherent resistance, primarily influenced by the shape of the collectors, as the airflow velocity increases. In order to assess the aerodynamic drag of the structure alone, additional tests

were performed on the model deprived of the electrodes. It should be noted that the positive convention is assumed for forces opposite to airflow direction, thus the aerodynamic resistance features a negative sign, while the generated thrust will contribute positively.

3.2.3. Electrical measurements. Electrical parameters such as corona voltage and corona current were measured to assess the thruster's power consumption and derive performance indicators. The voltage across the electrodes was measured using a purposely built voltage divider characterized by an output voltage ratio of $1/1000$ and a total resistance of 152.9 MΩ. The current flowing through the electrodes was measured by a contactless current probe, featuring a frequency range up to 120 MHz and an uncertainty of $\pm 1\%$. This kind of probe allows for a non-invasive measurement along the electrical circuit. Electric power is then calculated by multiplying the corona current i_c by the corona voltage V_c, therefore leading to a net measurement of the thruster's power consumption. Since, during the thruster's ignition, the current across the electrodes is in the order of 1 μA, a current multiplier was introduced by winding several turns of wire across the current probe, increasing its sensitivity. Then, a criterion for determining the ignition threshold was established: current values at voltages below 5 kV, where the thruster is assuredly off for this configuration, were averaged and the corresponding standard deviation was calculated (background noise). The threshold value was then set equal to the mean value increased by three times its standard deviation. This approach prevented any oscillations in the current value caused by noise to be interpreted as ignition values. For the ignition tests, the voltage has been slowly adjusted and ignition occurs as soon as the previous criterion is satisfied. The measurement is carried out multiple times, both while increasing and decreasing the voltage in order to get rid of any possible hysteresis.

The signals from all transducers were acquired with a sampling rate set to 2 kHz over a 5 s time window. The choice of these bandwidths takes into account that the generated EHD force, the aerodynamic loads and electrical quantities are close to stationary conditions. However, in the case of ignition and breakdown tests, an acquisition rate of 10 kHz was selected, in order to ensure a finer tracking of the corona voltage trend. This approach does not allow to capture the ns pulses typical of ignition and breakdown streamers, which are however of limited interest for the present study, that is aimed at studying the steady performance of the thruster.

4. Results

Wind tunnel tests involve speeds ranging from 0 to 12 m s^{-1} and corona voltages V_c from 0 to 20 kV, thus creating a test matrix.

The first results deal with ionic thrust, that being the difference between power on and off for each position in the test matrix. This also corresponds to the limit of an infinitely aerodynamic thruster assembly (where no drag is generated by the structure nor by the electrodes). The thrust vs convective velocity curve is a parabola with a negative second derivative, while being quadratic with respect to ΔV ($T \propto (\Delta V)^2$), where $\Delta V = V_c - V_i$ (the measured corona voltage V_c is equivalent to the applied voltage V_a used in the model section). Figure 9 shows the results for different corona voltages across the whole velocity range. Its quadratic trend is not easily discernible from the graph itself, however a parabolic fit proved to be much more accurate than a linear one.

The next parameter to be presented is the effective thrust (T_{eff}), which is the force felt by the load cell minus the drag of the frame that holds the electrodes. This is necessary as its shape, bulk and wind tunnel performance (as in blockage effect and interaction with boundary layers) is configuration dependent, meaningless for the investigation of the thruster itself. Preliminary tare tests allowed to exclude this extra drag and thus compensate for it. The effective thrust is a decreasing function of velocity, with a distinctively parabolic shape (figure 10). This is clearly an effect of the drag generated by the collectors themselves (and their mutual interaction), which is obviously a quadratic function of velocity. Since, as shown in the previous graph, the ionic thrust generated by the thruster is only slightly increasing with velocity, the increasing drag is clearly the dominant phenomenon (with respect to these particular collectors) and therefore the thruster will have a limiting velocity for its operation. This may be defined as the velocity for which the effective thrust becomes zero. The obvious conclusion is that the collectors will also have to be optimized for their dynamic performance, as opposed to the static tests that have been carried out so far. In the limit of an infinitely aerodynamic assembly of collectors (with a null aerodynamic drag), no limiting velocity is expected (at least for the incompressible speed regime). As for the static case, the generated thrust remains a quadratic function of voltage for each velocity.

In order to directly compare the results with the model, it is necessary to convert the experimental results into dimensionless coefficients. It is also necessary to scale the velocity using the notion of R_v, which is the non-dimensional velocity, retrieved as the ratio between convective and ionic velocity, as explained in the model section. The thrust coefficient C_T of the laboratory data is retrieved by dividing the thrust T/b by the reference value $\epsilon\eta(V_c - V_i)^2/d$ as in table 2, where V_i represents the ignition voltage and is a function of velocity, as shown later in section 4.1; this performance parameter is independent of corona voltage (as long as it is above ignition), while it varies with convective velocity. In order to compute the theoretical thrust, the model assumes a space-charge limited current (namely the 1D Mott-Gurney current when $v_b = 0$), to retrieve the corresponding charge density which is then multiplied by the electric field and integrated between the electrodes.

As explained in section 2, a new parameter η has been added to scale the reference electric field used to compute the dimensionless coefficients. This parameter affects both the values of the performance coefficients and that of the reference ionic velocity. The unmodified model ($\eta = 1$) would predict a shallower increase of thrust vs velocity with respect to

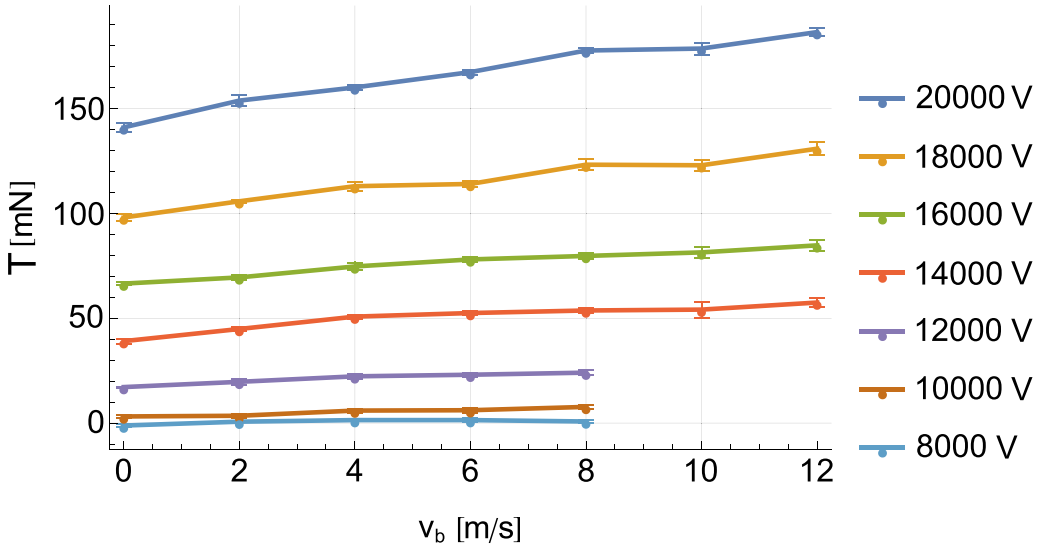

Figure 9. Ionic thrust.

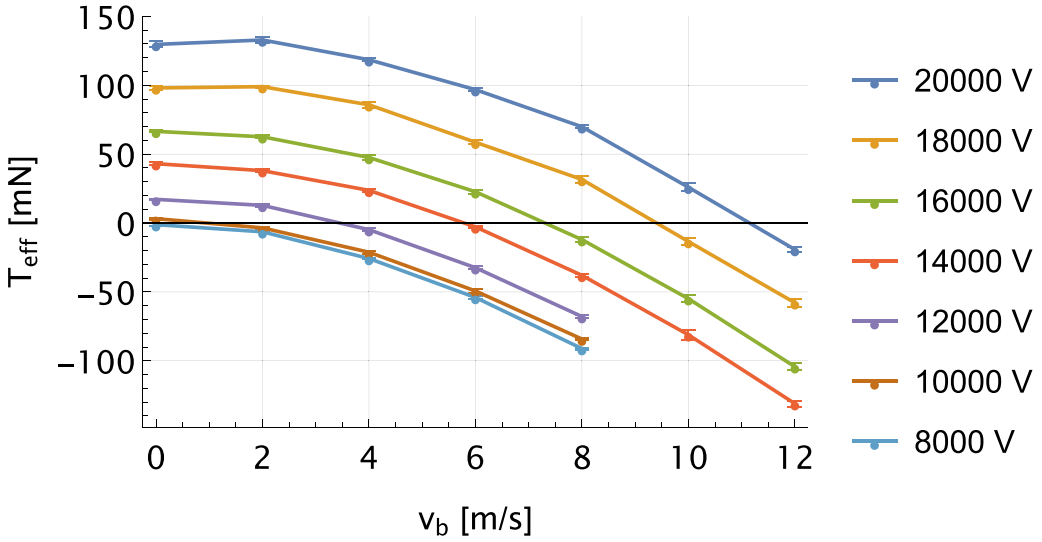

Figure 10. Effective thrust.

the experiment, as the different reference ionic velocity used to compute R_v would place the experimental results in the $0-0.06$ range, therefore placing their fit line considerably above the model line (the difference is shown in appendix). The concept of using a proper scaling parameter η will be referred to as 'horizontal rescaling' in following discussions, since it acts on the R_v scale.

All the following graphs of dimensionless quantities (figures 11, 13 and 15) use an $\eta = 0.22$, which shows an interesting agreement with the experimental results. The value of the extra parameter was chosen as a result of a fit (as a least squares problem) between the model's and the experimental line for the three dimensionless parameters. This has to be considered as an heuristic approach, driven by the obvious disparity in spatial dimensions between the 1D model and the 3D thruster, where the model is exploited to predict the trend with respect to a flow velocity change, rather than the absolute value of a given coefficient. However, the value of η does not reshape the model's curves, which retain their original trends and concavities.

In particular, figure 11 compares the measured thrust coefficient C_T (dots and red line) with the corresponding theoretical curve (blue line), i.e. the first section of the dimensionless thrust curve of figure 3, rescaled as explained above.

The corona current i_c instead increases with the convective velocity as a parabola with a positive second derivative, as shown in the model. This is confirmed by experimental results (figure 12). For a given velocity, corona current remains a quadratic function of ΔV.

In what follows (figure 13), the corona current is non-dimensionalized by computing the corresponding Mott–Gurney current and then diving by it the experimental data.

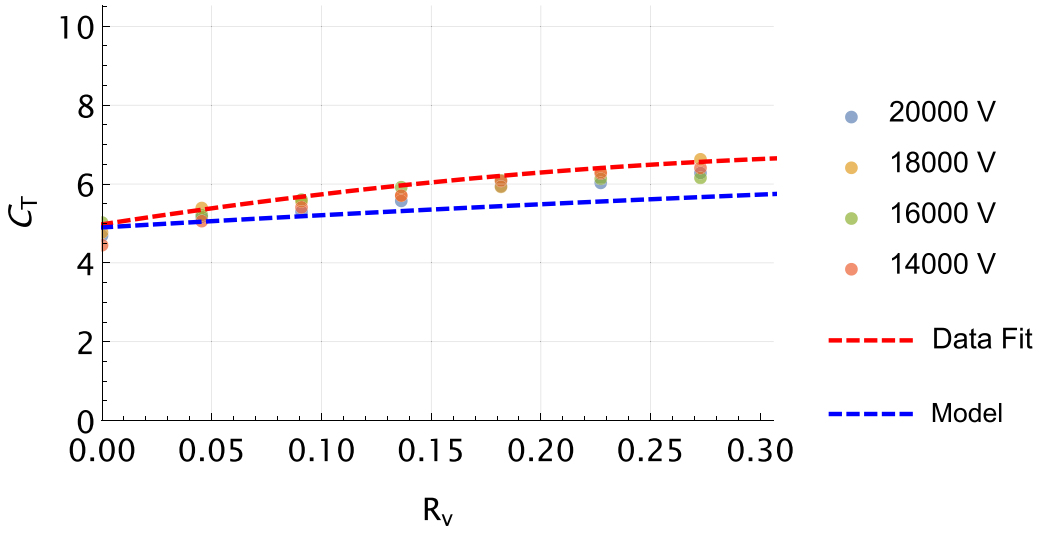

Figure 11. Experimental C_T vs rescaled model.

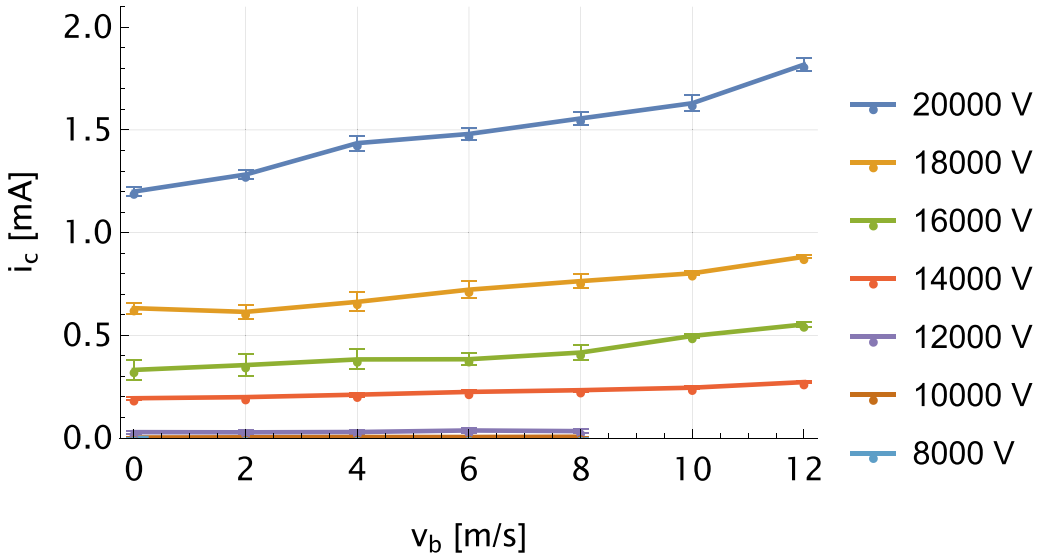

Figure 12. Corona current.

The model and the experimental data fit still show the same trend and concavity, thus confirming the model. The horizontal rescaling given by η is again necessary to achieve a satisfactory match between the two.

The main efficiency parameter of interest is the thrust-to-power ratio $\frac{T}{P}$. For a given velocity, this decreases with voltage as $\frac{1}{V}$, since thrust and electrical power are different powers of V (figure 14). For a given voltage above ignition, $\frac{T}{P}$ is instead a slightly decreasing function of velocity.

Its corresponding non-dimensional parameter (C_{TP}) is instead independent of voltage. There still is a dependency on convective velocity, in fact C_{TP} is, according to the model, a decreasing hyperbola of R_v with a positive second derivative. This entails a loss of efficiency as the convective velocity is increased, the obvious reason being the increased current density related to the convective velocity alone, which is only partially offset by the increase in thrust. While the experimental C_{TP} remains a decreasing function of velocity, the concavity is different from the theoretical one (figure 15). This may be explained by the fact that only a very small interval of velocities has been considered, with a dimensionless velocity R_v in the range $0-0.27$. Within those velocities the model predicts a very small concavity, albeit positive, while the experimental results show a slight negative one. Compared to the other parameters, this one involves an extra operation, that being the division between two different performance coefficients, thus suffering from higher uncertainties. The choice of $\eta = 0.22$ again improves the model's prediction.

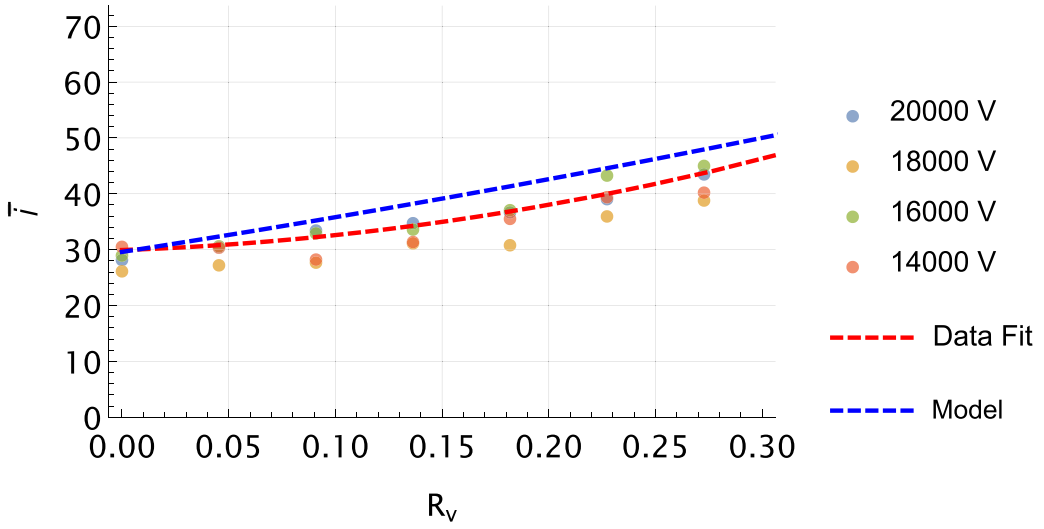

Figure 13. Experimental non-dimensional current vs rescaled model.

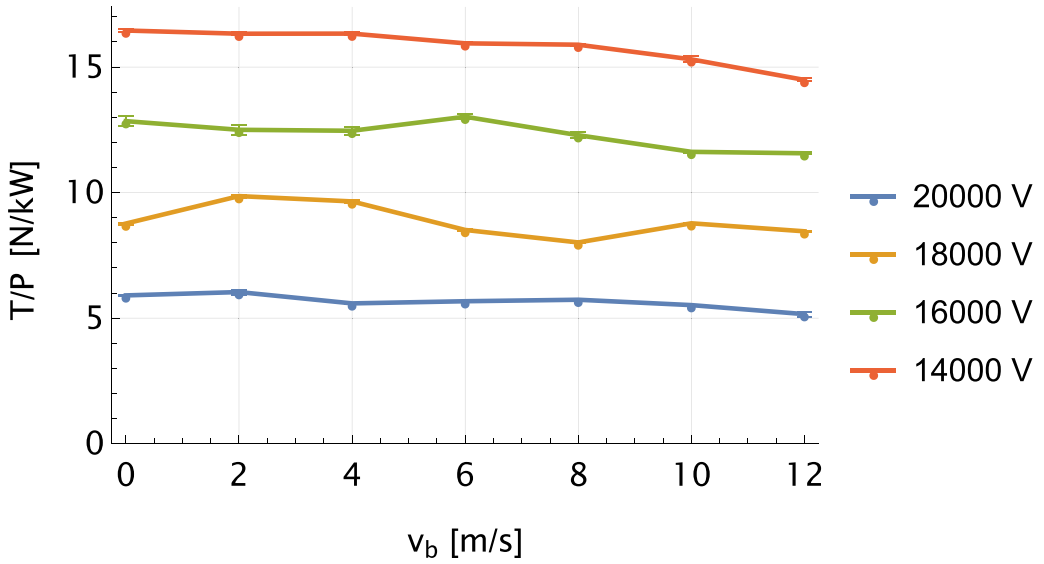

Figure 14. Thrust-to-power ($\frac{T}{P}$), computed using ionic thrust (T) from figure 9.

4.1. Effects of convective velocity on corona ignition and breakdown

Convective velocity also affects the operating voltage envelope of an ion thruster. In order to carry out the relative experiments, the setup had to be modified to accommodate a gap of 1 cm instead of the usual 2 cm. This was necessary because the expected breakdown voltage at 2 cm of gap was higher than the maximum for the available power supply unit, for coherence the same gap was used also for the ignition tests. All the tests have been carried out in conditions of stable temperature ($21 \pm 1\,^{\circ}$C), ambient pressure and humidity (RH $45 \pm 5\%$), which have been monitored throughout the tests. A change in these parameters (humidity in particular) could possibly affect both the ignition and breakdown voltages but its impact has not been assessed in this study. Experiments showed that an increasing convective velocity decreases the required ignition voltage while increasing the breakdown voltage [37], thus expanding the operating envelope and therefore increasing the theoretical maximum thrust production (which is an increasing quadratic function of $\Delta V = V_c - V_i$). While the trends of all performance parameters have been theoretically estimated first and then tested experimentally, the varying envelope does not possess an underlining physical explanation, since the drift region modelling lacks by nature the ion production mechanism, which is of paramount importance for both corona ignition and breakdown. A model for the ionization region would then be necessary to explain this phenomenon, for which only the experimental results are here provided (figure 16).

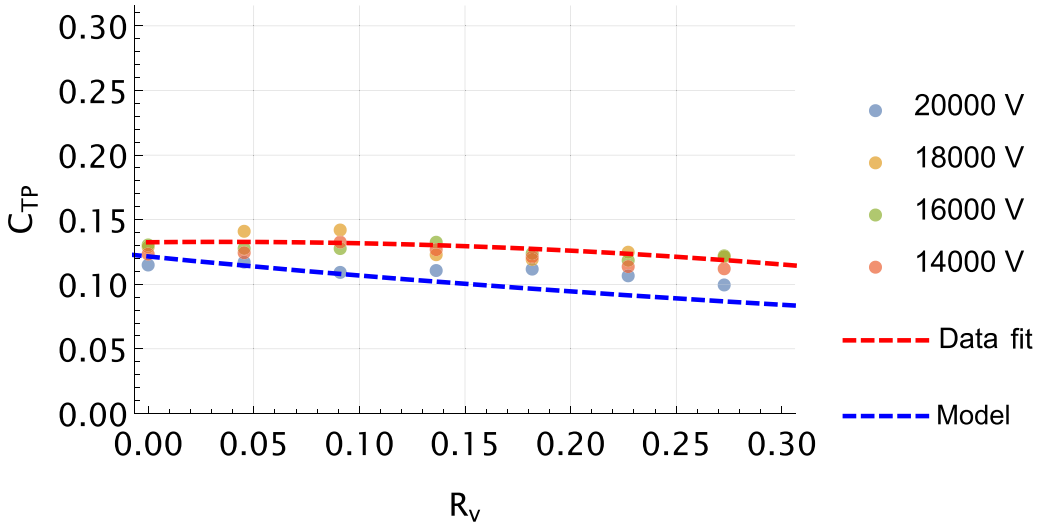

Figure 15. Experimental C_{TP} vs rescaled model.

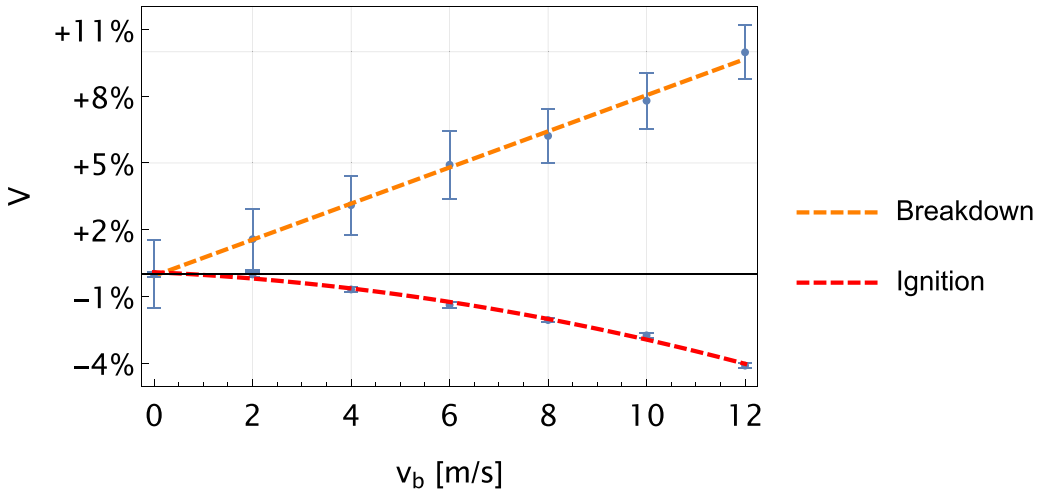

Figure 16. Voltage envelope.

Specifically, the ignition voltage decreases as a quadratic function of velocity, albeit with a small first derivative thus not greatly affecting the absolute ignition voltage value, which decreases by about 4% in the considered speed range.

The breakdown voltage instead increases linearly with velocity, with a higher derivative. An increase of about 10% has been observed in the same speed range. The higher uncertainties related to the breakdown voltage (which represent the standard deviation across multiple tests) are related to the nature of the experiment itself, which is affected by a series of external factors. In fact, breakdown tests are destructive tests, that microscopically modify both electrodes when an electric arc is formed, therefore changing the local electric field shape and therefore the required breakdown voltage. This drawback has been overcome by periodically rebuilding the setup and performing a sufficiently high number of tests until statistical convergence is reached, which in this case corresponds to having a clear trend of breakdown voltage with respect to velocity (here discovered to be linear).

Using the experimental C_T from the previous section it is also possible to retrieve the theoretical maximum thrust (obtained just below breakdown voltage and considering the expanding ΔV) for each velocity (figure 17). Results show that maximum thrust increases by about 80% in the considered speed range, both due to the increasing thrust coefficient and the expanding operating voltage envelope. Its trend appears to be quadratic, albeit with a very small positive concavity.

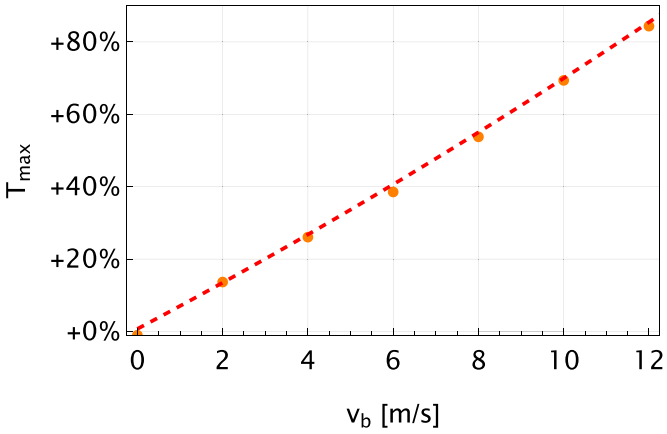

Figure 17. Maximum achievable ionic thrust.

5. Discussion and conclusions

The results collected in this article confirm that an EHD thruster may be employed also outside quasi-static conditions and could therefore be taken into account for a series of atmospheric applications, albeit in the incompressible regime. The maximum ionic thrust that can be provided by the thruster is an increasing function of velocity, even though its effective thrust would be decreased by the aerodynamic drag of the electrodes. However, since the maximum achievable ionic thrust is also a parabola, just like the aerodynamic drag, it should be in theory possible to design a thruster whose drag coefficient is low enough that also the effective thrust will not decrease with velocity. Therefore, if an EHD thruster requires to be employed in non-static conditions, it should be designed with the lowest possible drag coefficient in mind. This obviously points towards smaller and thinner collectors, which would not be optimal at zero velocity, but would become better as soon as the velocity is increased, even to modest values such as those considered in this test campaign. In order to take full advantage of the increased performance of the thruster with increasing convective velocity, the input voltage should be increased accordingly so to exploit the expanding operating envelope, which in turn would mean oversizing the required power supply unit, as it should be possible to go above the breakdown voltage for the static case.

The results agree with the general trend already discussed in the almost concurrent work [36], such as confirming a decreasing effective thrust with velocity (while operating at fixed voltage) and an increasing corona current. The extra accuracy granted by the direct thrust measurement employed in the present article allowed to disclose also higher derivatives of the performance parameters and link them, for the first time, to a complete physical model of the drift region.

This article also redefines the performance coefficients to better address the voltage characteristics of an EHD thruster and better fit the experimental results. An extra parameter (η) is also introduced to scale the dimensionless coefficients and better fit the experimental results with the model. This parameter adjusts the reference electric field used in all computations.

Future developments would therefore require testing at higher velocities, closer to the ionic velocity and the compressible regime, in order to discover the actual peak in ionic thrust. The model would then require to be adapted to the compressible regime, with the possibility of this requiring a numerical solution. Additional test campaigns would also be needed to find new optimal geometries for a thruster operating at a given velocity.

Data availability statement

The data that support the findings of this study are openly available at the following URL/DOI: https://doi.org/10.5281/zenodo.12582553.

Acknowledgments

This project has received funding from the European Union's Horizon Europe Research and Innovation Programme under Grant Agreement No 101098900. Views and opinions expressed are however those of the authors only and do not necessarily reflect those of the European Union or European Innovation Council and SMEs Executive Agency (EISMEA). Neither the European Union nor the granting authority can be held responsible from them.

Appendix

As clearly visible in figure 18, the effect of η is mainly that of a horizontal rescaling, on top of a vertical multiplication. This can be explained considering the different reference ionic velocity (and therefore R_v) that result from the choice of η. It is therefore probable that the actual (and most representative for thrust production) reference ionic velocity is lower than that traditionally obtained using the average electric field.

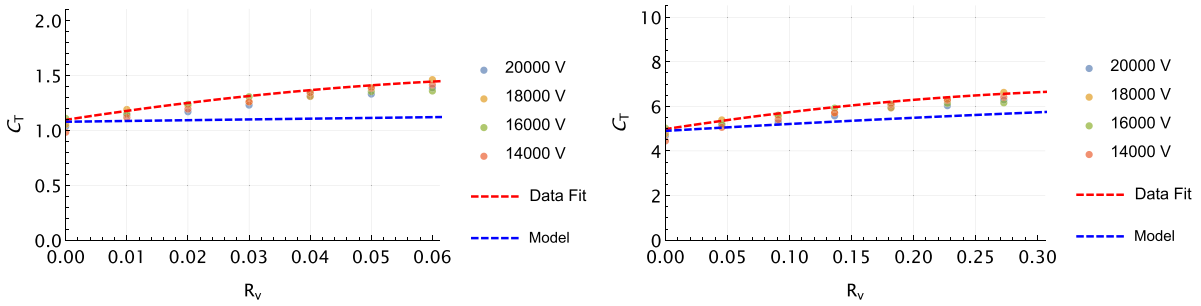

Figure 18. $\eta = 1$ (left) vs $\eta = 0.22$ (right).

ORCID iDs

Stefano Trovato https://orcid.org/0000-0002-1479-4572
Raffaello Terenzi https://orcid.org/0000-0002-3126-1786
Davide Usuelli https://orcid.org/0000-0003-2910-9053
Marco Belan https://orcid.org/0000-0001-7040-0286

References

[1] Goebel D M and Katz I 2008 *Fundamentals of Electric Propulsion: Ion and Hall Thrusters* (Wiley)
[2] Mazouffre S 2016 *Plasma Sources Sci. Technol.* **25** 033002
[3] Charles C 2009 *J. Phys. D: Appl. Phys.* **42** 163001
[4] Cao W, Mecrow B C, Atkinson G J, Bennett J W and Atkinson D J 2012 *IEEE Trans. Ind. Electron.* **59** 3523–31
[5] Brelje B J and Martins J R R A 2019 *Prog. Aerosp. Sci.* **104** 1–19
[6] Moreau E, Benard N, Lan-Sun-Luk J-D and Chabriat J-P 2013 *J. Phys.* D **46** 475204
[7] Xu H, He Y, Strobel K, Gilmore C, Kelley S, Hennick C, Sebastian T, Woolston M, Perreault D and Barrett S 2018 *Nature* **563** 532–5
[8] Townsend J 1914 *London, Edinburgh Dublin Phil. Mag. J. Sci.* **28** 83–90
[9] Peek F 1920 *Dielectric Phenomena in High Voltage Engineering* (McGraw-Hill, Inc.)
[10] Robinson M 1962 *Am. J. Phys.* **30** 366–72
[11] Loeb L 1965 *Electrical Coronas, Their Basic Physical Mechanisms* (University of California Press)
[12] Christenson E and Moller P 1967 *AIAA J.* **5** 1768–73
[13] Bahder T and Fazi C 2003 *Force on an Asymmetric Capacitor* (Army Research Laboratory)
[14] Kiousis K, Moronis A and Fruh W 2014 *Plasma Sci. Technol.* **16** 363
[15] Khomich V and Rebrov I 2018 *J. Electrostat.* **95** 1–12
[16] Kahol O, Belan M, Pacchiani M and Montenero D 2023 *J. Electrostat.* **123** 103815
[17] Belan M, Arosti L, Polatti R, Maggi F, Fiorini S and Sottovia F 2021 *J. Electrostat.* **113** 103616
[18] Xu H, Gomez-Vega N, Agrawal D and Barrett S 2019 *J. Phys.* D **53** 025202
[19] Belan M, Terenzi R, Trovato S and Usuelli D 2022 *J. Electrostat.* **120** 103767
[20] Lemetayer J, Marion C, Fabre D and Plouraboué F 2022 *J. Phys. D: Appl. Phys.* **55** 185203
[21] Arif S, Branken D J, Everson R C, Neomagus H W J P and Arif A 2018 *J. Electrostat.* **93** 17–30
[22] Vega N, Xu H, Abel J and Barrett S 2021 *Appl. Phys. Lett.* **118** 074101
[23] Xu H, He Y and Barrett S 2019 *Appl. Phys. Lett.* **114** 254105
[24] Orrière T, Moreau E and Pai D Z 2019 *J. Phys. D: Appl. Phys.* **52** 464002
[25] Lacoste D, Pai D and Laux C 2004 *Ion Wind Effects in A Positive DC Corona Discharge in Atmospheric Pressure Air* (American Institute of Aeronautics and Astronautics)
[26] Masuyama K and Barrett S 2013 *Proc. R. Soc.* A **469** 20120623
[27] Wilson J, Perkins H and Thompson W 2009 An investigation of ionic wind propulsion *Technical Report* NASA/TM-2009-215822 NASA
[28] Belan M, Baldo J, Kahol O and Montenero D 2024 *J. Phys. D: Appl. Phys.* **57** 195201
[29] Kaci M, Said H A, Laifaoui A, Aissou M, Nouri H and Zebboudj Y 2015 *Braz. J. Phys.* **45** 643–55
[30] Ieta A and Chirita M 2019 *J. Electrostat.* **100** 103352
[31] Drew D and Follmer S 2021 High force density multi-stage electrohydrodynamic jets using folded laser microfabricated electrodes *21st Int. Conf. on Solid-State Sensors, Actuators and Microsystems (Transducers, New York) (Inst. of Electrical and Electronics Engineers)* pp 54–57
[32] Chirita M and Ieta A 2022 *J. Propuls. Power* **38** 893–900
[33] Gilmore C K and Barrett S R H 2018 *AIAA J.* **56** 1105–17
[34] Gomez-Vega N, Brown A, Xu H and Barrett S 2023 *AIAA J.* **61** 767–79
[35] Guerra-Garcia C, Nguyen N, Mouratidis T and Martinez-Sanchez M 2020 *J. Geophys. Res: Atmos.* **125** e2020JD032908
[36] Grosse S, Benard N and Moreau E 2024 *J. Electrostat.* **130** 103950
[37] Messanelli F, Frigerio E, Tescaroli E B M and Belan M 2019 *Exp. Therm. Fluid Sci.* **105** 123–35